11.6 NUMERICAL SIMULATIONS OF COASTAL WIND EVENTS IN THE NORTH GULF OF ALASKA

Peter Q. Olsson*
Karl P. Volz
Han Yi
Alaska Experimental Forecast Facility, University of Alaska Anchorage, Anchorage, Alaska

1. INTRODUCTION

From the meteorological perspective, the Gulf of Alaska is a region of extremes. The northern Gulf of Alaska experiences the potent consequences of vigorous marine extratropical cyclones making landfall in some of the most dramatic and extreme terrain in North America. The high frequency of storms— on average one every four to five days during the cold season (Hartman 1974)— often create strong pressure gradients that interact with local topography to produce localized wind regimes in strong contrast to the larger scale circulation.

These winds often take the form of strong ageostrophic low-level jets (LLJs) that present a significant hazard to local aviation and marine interests (e.g., Macklin et al. 1990, Bond and Macklin, 1993). Such LLJs are of particular concern since they often occur on a smaller scale than is accurately represented in the current suite of operational numerical weather prediction (NWP) models. There is a temporal scale issue in numerically forecasting these winds as well— such LLJs may develop and dissipate on time scales (O(2 h)) less than that currently represented by the NWP output typically available to the forecaster. Currently, the forecasting of these localized wind events must be done from a consideration of larger-scale forecast pressure patterns and the forecaster's personal knowledge of complex pressure gradient/topography interactions.

The intent of this study is to determine the utility of high-resolution NWP in actually forecasting the wind events themselves. Along the North Gulf of Alaska coast verification of such simulations is difficult due to the paucity of surface and upper-air observations. Here, we use Synthetic Aperture Radar (SAR)-derived wind retrievals to provide an observed snapshot of surface wind conditions. A comparison with concurrent high resolution NWP output is used to determine the skill of the model run at various resolutions in simulating observed LLJ cases.

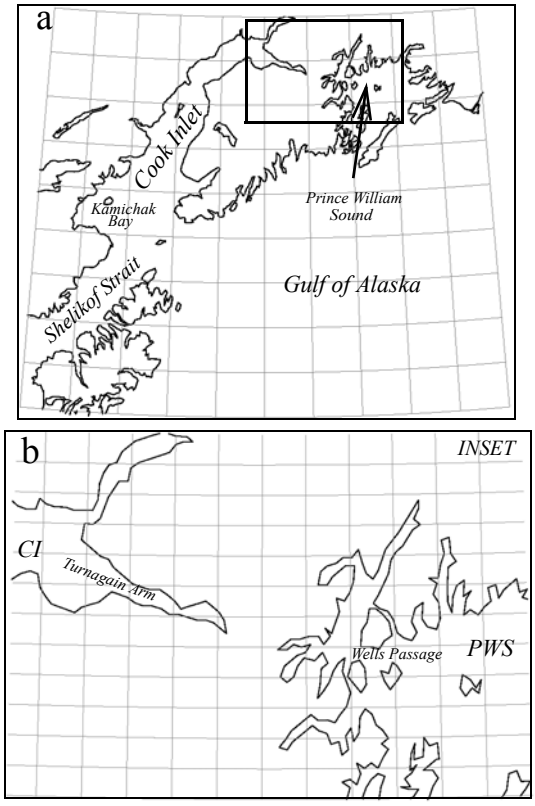

Fig. 1. a) The North Gulf of Alaska, and b) close-up of Upper Cook Inlet and Prince William Sound (see location of inset in a).

2. GULF OF ALASKA COASTAL TOPOGRAPHY

While Prince William Sound (PWS) and Cook Inlet (CI) are only a small part of the Gulf of Alaska Coast

* *Corresponding author address*: Peter Q. Olsson, Alaska Experimental Forecast Facility (AEFF), University of Alaska Anchorage, 2811 Merrill Field Dr., Anchorage, AK 99501. olsson@aeff.uaa.alaska.edu

(Fig. 1), they experience most of the weather features and phenomena seen in the rest of the Gulf. During the winter storm season, strong atmospheric pressure gradients occur across this region as cyclones transit the northern Gulf. PWS is a complex embayment composed of fjords, deeply incised river valleys, and steep mountain ridges. Much of PWS is surrounded by the Chugach Mountains, that here average about 2000 m in elevation, with peaks extending to near 3000 m. There are three significant gaps in the terrain that can act to funnel and focus regional winds. Each of these gaps has the potential to permit exchange of air with a considerably different, and often continental, air mass (Macklin et al. 1988). By contrast, Cook Inlet (CI), lying just to the west of PWS is a long estuary forking into two orthogonal fjords— Knik and Turnagain Arms— at its upper terminus, with the City of Anchorage located at the joining of the arms. Cook Inlet is bounded on the west by the massive Aleutian Range and on the east by the Kenai Peninsula.

3. SAR WINDS

While LLJs are well known to mariners and general aviation, lack of quantitative observations present a significant challenge to studying LLJs along the Gulf coast. One tool that has recently become available over water is Synthetic Aperture Radar (SAR) derived winds. In this technique, satellite observations of the surface sea state are combined with approximations of wind direction to infer wind speed. While still considered experimental, SAR-derived winds provide an unprecedented snapshot of surface winds (such as LLJs) over water at resolutions down to 400 m in scale (see http://orbitnet.nesdis.noaa.gov/orad/sar).

4. NUMERICAL MODEL

The numerical model used for this study is the *R*egional *A*tmospheric *M*odeling *S*ystem (RAMS), a nonhydrostatic primitive-equation finite-difference model that includes parameterizations for mixed-phase microphysics, radiation, and planetary surface processes.

Central to the versatility of RAMS is a multiple grid nesting scheme that permits solution of the primitive equations simultaneously on several meshes of differing spatial resolution. This is useful in the current application, since the pressure gradients that force LLJs on the scale of several kilometers result from fluid dynamical processes that occur on the scales of hundreds to thousands of kilometers.

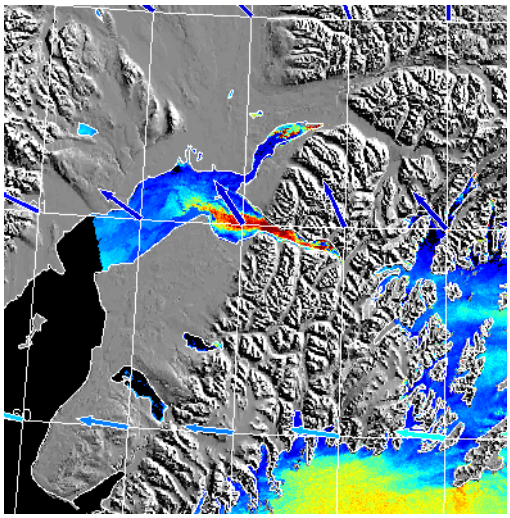

Fig. 2. The Turnagain Arm jet of 01/17/02, 2:48Z. The color bar for the wind speeds is the same as that of Fig 3. Note that since the wind speed is derived from sea surface wave characteristics, the signal over land is masked out.

The key questions addressed by this study are:

- Do the numerical simulations reproduce the SAR-derived winds, and
- If so, what grid resolution is necessary to reproduce the observed results, and,
- Can LLJs themselves (vs. the large-scale conditions that cause them) feasibly be forecast locally/regionally using a cluster of workstations and a parallel NWP model?

This last point is significant because the direct forecasting of LLJs by the NWP model allows non-specialists to use the model-derived graphics directly without the intermediate intervention of a trained forecaster. This last point also bears on the ability/utility of a fine-mesh NWP model to provide an upper boundary condition for a high-resolution oceanographic prediction model such as may be used to predict plume dispersion in the event of an oil spill.

For the sensitivity study shown here, several grid configurations are used, depending on the situation being simulated. In all simulations, the coarse grid and at least one nested grid are employed (64 km and 16 km

grid spacing respectively). As the key terrain features in the regions of interest often have a characteristic length scale *O*(1 km), a finer- mesh grid (grid 3 at 4 km spacing) was employed in most cases. In 2 of the 3 cases presented here simulations implementing a fourth very high resolution gird with a 1 km mesh were also tested. All of the simulations were performed using the parallel version of RAMS on a 24-node workstation cluster.

5. RESULTS

5.1 The Turnagain Arm Jet, 17 Jan, 2002

The Turnagain Arm Jet is a fairly common easterly wind feature that extends from the upper Turnagain Arm (see location in Fig 1b) westward towards the main body of upper Cook Inlet.A strong example of this jet can be seen in the SAR image in Fig. 2. This typically

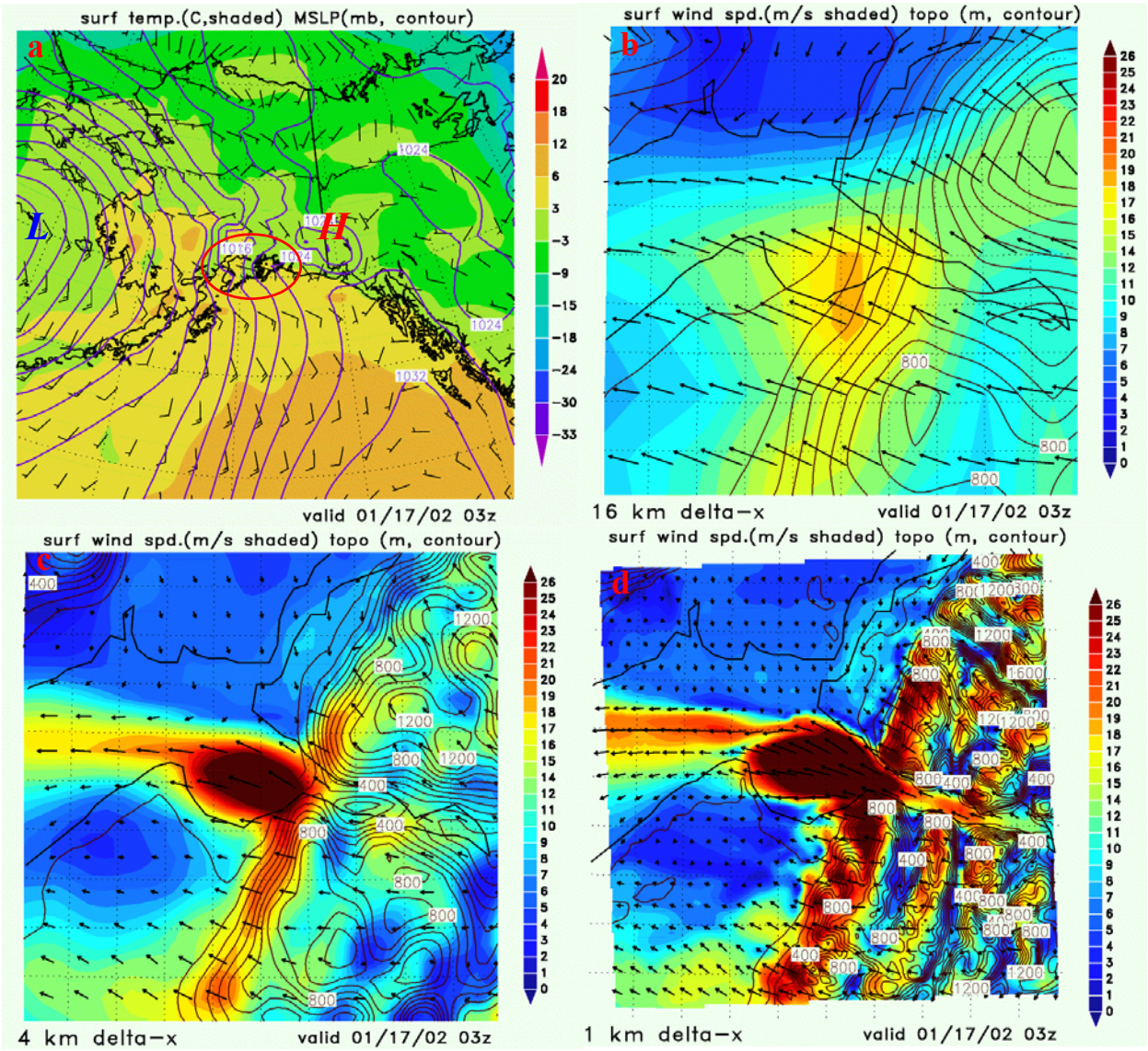

Fig. 3. a) The large-scale pressure and temperature patterns for 01/127/02 at 03z. The red oval denotes the area of PWS/CI area of interest. b) Surface wind speed (m s^{-1}) and direction (vectors) and topography contours for a 2 grid simulation (finest grid at 16-km Δx). c) Surface wind speed and direction and topography contours for a 3 grid simulation (finest grid at 4-km Δx). c) Surface wind speed and direction and topography contours for a 4 grid simulation (finest grid at 1-km Δx)

results from a large-scale pressure gradient with a strong zonal component such as that seen in Fig. 3a, which shows a deep low over the Bering Sea and a high to the east of PWS. (Note that the region of specific interest is denoted by the red oval). The simulated local pressure gradient along the axis of Turnagain Arm is greater that

4 mb over a distance of 75 km. Panels b, c, and d in Fig 3 show increasingly higher grid-resolution simulations at 16, 4, and 1 km Δx respectively.

The model topography is contoured these plots. At 16 km grid spacing, upper Turnagain Arm is represented as essentially a hanging valley. The surface winds show a maximum of about 18 m s^{-1} in Turnagain Arm, in what appears more like a lee-wave structure than a LLJ. At 4 km Δx, (Fig 3c) the relatively wide mouth of lower Turnagain Arm is fairly well represented in the topography and contains a wind speed maximum of over 25 m s^{-1}, somewhat greater than the speed seen in the SAR wind retrieval in Fig 2. On the 1-km Δx grid (Fig. 3d) virtually the entire channel of Turnagain Arm is represented at sea level and the LLJ extends back well into the upper Arm.

5.2 The Wells Passage Jet, 20 Feb, 2002.

When the large-scale pressure gradient is in the generally opposite sense to that in Fig. 3a (i.e, with lower pressure to the east), a westerly jet similar in nature to the Turnagain Jet forms in Wells Passage, a fjord and channel system just to the east of Turnagain Arm on the northwest margin of PWS (see location in Fig 1b). Figure 4 shows the large-scale surface conditions at 3 Z on 02/20/02. A surface low sits just to the east of PWS with a ridge of high pressure to the west on the west side of the Aleutian Range. Such conditions often create a strong pressure gradient and associated LLJ on the western margins of PWS.

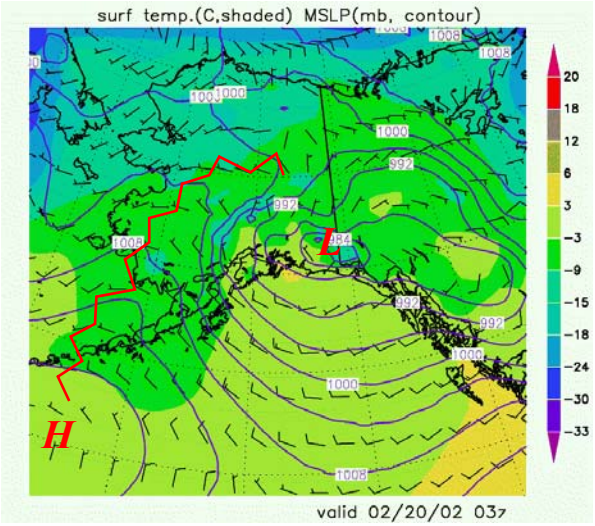

Fig. 4. The large-scale surface temperature mean sea-level pressure and winds. Also shown is the shortwave ridge rotating around the high south of the Alaska Peninsula Pressure contours are 4 mb intervals.

Figure 5a shows a concurrent SAR image where the Wells Passage Jet can be seen extending through the Passage well into the center of PWS with maximum winds in excess of 25 m s^{-1}. Figure 5b shows the results of a 2-grid simulation with a fine grid of 16 km Δx. As in the Turnagain Arm case at the same grid spacing, the channel is not resolved in the model topography. This being the case, the LLJ is only hinted at in the plot with a broad wind maximum of 17 m s^{-1} in the open Sound to the east of Wells Passage.

At 4 km Δx (Fig. 5c), the actual Passage is marginally resolved in the topography, though more as a broad above sea-level valley encompassing Wells Passage, Port Nellie Juan to the south, and the island mass separating them. Two wind maxima of about 19 m s^{-1} are in evidence at the head of Passage Canal (bay to the west of Wells Passage) and another over the islands to the south of Wells Passage. Again these maxima appear to be more like lee waves. At 1 km Δx (Fig. 5d), the channel is well resolved and a LLJ with maximum speeds in excess of 23 m s^{-1} is in clear evidence throughout the Passage Canal extending eastward to central PWS. This figure compares favorably with the SAR image in Fig. 5a both in extent and magnitude, with the SAR-derived winds about 10% greater in magnitude.

5.3 The Iliamna Jet, 12 Mar., 2002

The westerly Iliamna Jet, originating in Kamishak Bay, and extending over the Barren Islands into the northwest Gulf of Alaska, is one of the best studied LLJs in the CI/PWS region (Macklin et al. 1990). This wind feature occurs when a strong east-to-west pressure gradient exists over lower CI and the pass separating Lake Iliamna and Kamishak Bay. A good example of this jet can be seem in the SAR image of 3 Mar. 2002 in Fig. 6a with winds speeds exceeding 22 m s^{-1}. On this day a 975 mb low is positioned off the coast of the southeast panhandle of Alaska. A high pressure ridge extends northward over the Alaska Peninsula and Bristol Bay in the Bering Sea. This LLJ is fairly common and is a significant hazard to marine traffic traversing the Cook Inlet marine corridor.

Figure 6c shows the results of a 2-grid (16 km Δx) simulation of the jet. Unlike the other cases where the

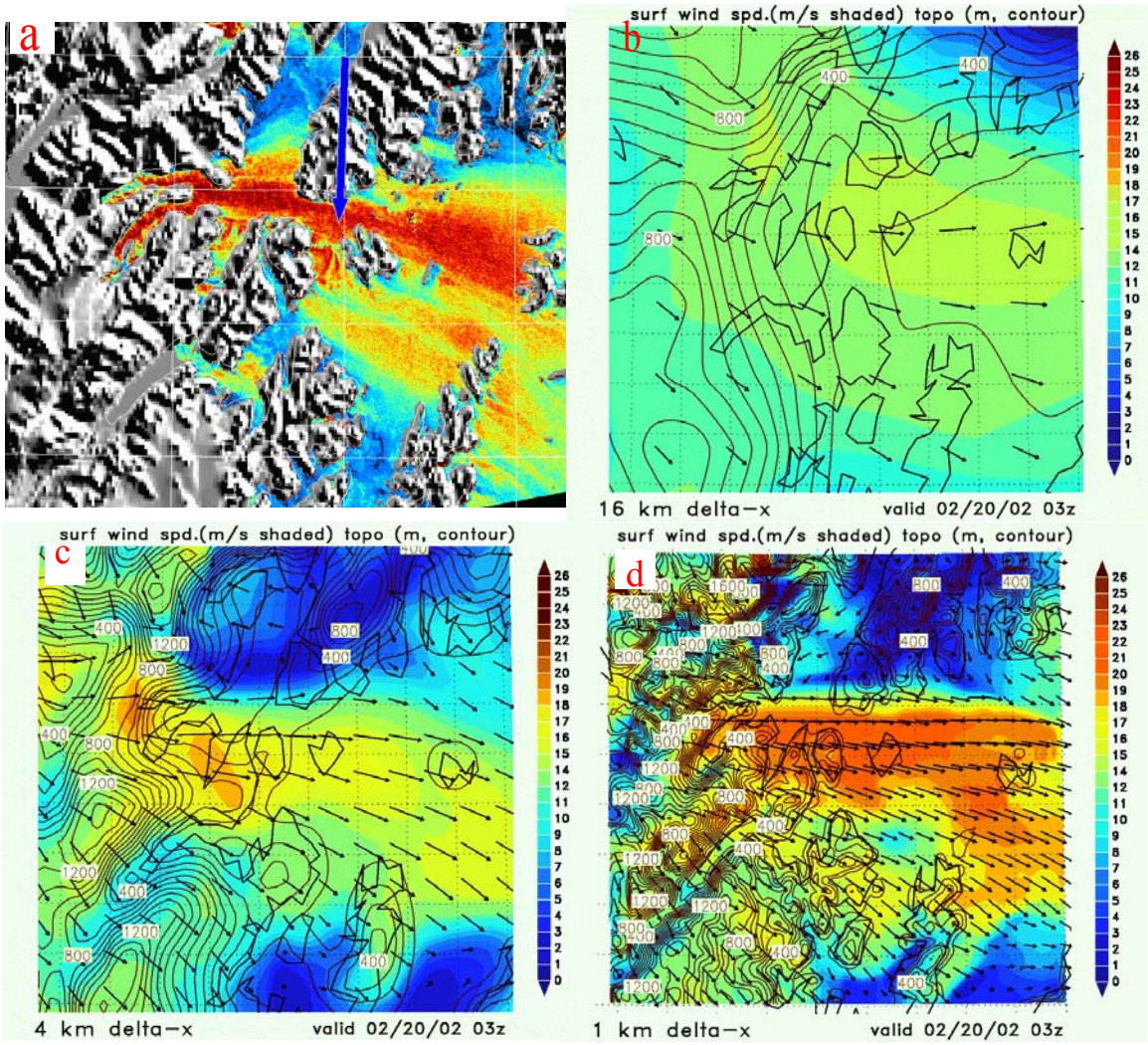

Fig. 5. a) SAR image of the Wells Passage Jet of Feb 20, 2002 (color key same as in panel b to the right) with maximum wind speeds in excess of 25 m s^{-1}. b) Surface wind speed (m s^{-1}) and direction (vectors) and topography contours for a 2 grid simulation (finest grid at 16-km Δx). c) Surface wind speed and direction and topography contours for a 3 grid simulation (finest grid at 4-km Δx). d) Surface wind speed and direction and topography contours for a 4 grid simulation (finest grid at 1-km Δx)

jet is poorly resolved at this grid spacing, the LLJ here is clearly in evidence, though the speed maximum is only about 18 m s^{-1}. As this jet is of much larger extent (width of ~80 km), this is not too surprising. (Note that the topography defining the gap is quite well resolved at this resolution) Figure. 6d shows concurrent results from a 4 km Δx simulation of the Iliamna Jet. Here the maximum wind speed is about 25 m s^{-1}. This figure agrees quite well with the SAR image, including the second smaller LLJ (the "Kuguyak Jet") also visible to between the mainland and Kodiak Island in northern Shelikof Strait, to the south of the Iliamna Jet. A 1 m Δx run was performed for this case (not shown). It produced results nearly identical to the 4 km Δx results shown here.

6. DISCUSSION

In the preceding section results of several simulations of LLJs in the CI/PWS region of the Gulf of Alaska are presented. In all three cases, it was found possible to simulate the observed LLJs given sufficiently fine grid resolution. Though wind speeds at the highest resolution in some cases were greater than those observed in the SAR retrievals and in others it somewhat less, the model was able to obtain a wind speed distribution close to the SAR observations.

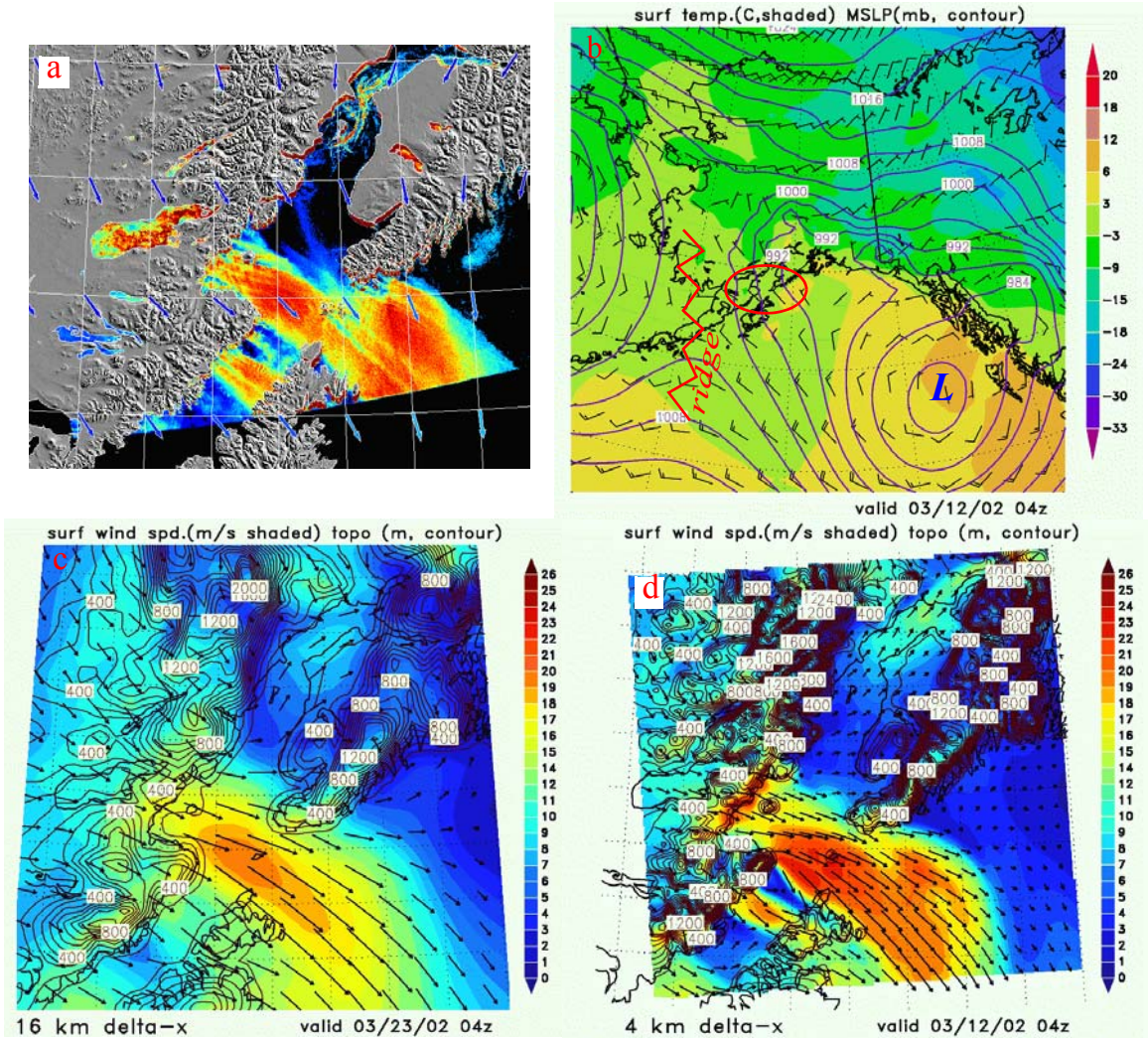

Fig. 6. a) A SAR image of surface winds on 3 Mar. 2002 at 3:48Z (color bar same as in panel c). b) Large-scale temperature and pressure fields at 4Z on the same day. Red oval denotes the area of interest. c) Surface wind speed and direction and topography contours for a 2 grid simulation (finest grid at 16-km Δx). d) Surface wind speed and direction and topography contours for a 3 grid simulation (finest grid at 4-km Δx)

As noted in the proceeding section, the resolution of the model topography varies with grid spacing—increasing grid resolution permitting more realistic topography for each case. This improved terrain resolution was seen to correlate well with improved results, in particular with higher wind speeds that agreed better with the observations. This begs the question: "Does the model do better at small grid spacings because of better topography or because the dynamics of the fluid at small scales is better represented"?

To test this, we performed a series of simulations in which the finest grid had topography interpolated from its parent grid. In this way we can, for example, run a 4 km Δx simulation with the same topographic representation used at 16 km Δx. In most cases, it was found that the results were similar to the coarser-resolution run in terms of wind speed distribution with the speeds somewhat higher at the greater grid resolution. This suggests that the representation of the topography is a significant factor in the increasingly better results with decreasing grid spacing.

Given the results shown above, we address the final question: "Is it feasible to use a locally run high-resolution NWP model operationally to actually predict LLJs?" Our results suggest that the answer to this ques-

tion depends on the scale of the jet and/or the scale of the channeling topography.

As currently implemented, the forecast version of RAMS as run at the Alaska Experimental Forecast Facility (AEFF) produces a 36 h forecast for PWS and upper CI at 4 km Δx in about 3.5-4 h. Clearly, the Iliamna Jet, which is even fairly well resolved at 16 km Δx, would be well represented in such a model configuration. Similarly, the Turnagain Arm Jet is quite apparent at 4 km Δx (Fig. 3c), at least near the confluence of the Arm with CI. From this result, the existence of the LLJ in the upper Arm can reasonably be inferred, though it is not actually present in the simulation. The Wells Passage Jet is the least well represented at 4 km Δx. While a weak LLJ is apparent at the 4 km Δx resolution, it is much weaker than the observed and 1 km Δx cases. Such a fine scale is not currently practical for a forecast NWP model. However, computer hardware continues to increase in performance, suggesting that forecasting on the 1 km scale— at least on a fairly limited domain— may become possible in the not-to-distant future.

7. CONCLUDING REMARKS

From a forecast perspective, this study has several implications. For short-term mesoscale marine weather forecasts, the better resolution of localized winds is clearly worth the extra computational expense required for the 4-km grid. While the configuration of the 1-km grid is not currently feasible to run as an operational forecast model, it clearly is required to adequately resolve some localized low-level jets, and the next generation of computers will make this kind of prediction possible on an operational basis.

ACKNOWLEDGEMENTS

This work was supported by a grant from the Oil Spill Recovery Institute (OSRI), Cordova, Alaska. The authors would like to thank NOAA/NESDIS and Johns Hopkins University/Applied Physics Laboratory for the use of SAR images shown here.

REFERENCES

Bond, N.A., and S.A. Macklin, 1993: Aircraft observations of off-shore directed flow near Wide Bay, Alaska. *Mon. Wea. Rev.*, 121, 150-161.

Hartmann, D.L., 1974: Time spectral analysis of mid-latitude disturbances. *Mon. Wea. Rev.*, 102, 348-362

Macklin, S. A., N. A. Bond, and J. P. Walker, 1990: Structure of a low-level jet over lower Cook Inlet, Alaska. *Mon. Wea. Rev.*, 118, 2568-2578.

Macklin, S.A., G. M. Lackman, and J. Gray, 1988: Offshore-directed winds in the vicinity of Prince William Sound, Alaska, *Mon. Wea. Rev.*, 116, 1289-1301.